



UNIVERSITY OF LEEDS

This is a repository copy of *Markerless attenuation correction for carotid MRI surface receiver coils in combined PET/MR imaging.*

White Rose Research Online URL for this paper:
<http://eprints.whiterose.ac.uk/86886/>

Version: Accepted Version

Article:

Eldib, M, Bini, J, Robson, PM et al. (4 more authors) (2015) Markerless attenuation correction for carotid MRI surface receiver coils in combined PET/MR imaging. *Physics in Medicine and Biology*, 60 (12). 4705 - 4717. ISSN 0031-9155

<https://doi.org/10.1088/0031-9155/60/12/4705>

Reuse

Unless indicated otherwise, fulltext items are protected by copyright with all rights reserved. The copyright exception in section 29 of the Copyright, Designs and Patents Act 1988 allows the making of a single copy solely for the purpose of non-commercial research or private study within the limits of fair dealing. The publisher or other rights-holder may allow further reproduction and re-use of this version - refer to the White Rose Research Online record for this item. Where records identify the publisher as the copyright holder, users can verify any specific terms of use on the publisher's website.

Takedown

If you consider content in White Rose Research Online to be in breach of UK law, please notify us by emailing eprints@whiterose.ac.uk including the URL of the record and the reason for the withdrawal request.



eprints@whiterose.ac.uk
<https://eprints.whiterose.ac.uk/>

*Markless Attenuation Correction for Carotid MRI Surface Receiver Coils in
Combined PET/MR Imaging*

Mootaz Eldib, M.Sc.^{1,2}, Jason Bini, M.Sc.^{1,2}, Philip M. Robson, Ph.D.^{1,3}, Claudia
Calcagno, M.D., Ph.D.^{1,3}, David D. Faul, Ph.D.⁴, Charalampos Tsoumpas^{1,5}, Zahi A.
Fayad, Ph.D.^{1,3,6}

¹Translational and Molecular Imaging Institute, Icahn School of Medicine at Mount
Sinai, New York, NY

²Department of Biomedical Engineering, The City College of New York, New York, NY

³Department of Radiology, Icahn School of Medicine at Mount Sinai, New York, NY

⁴Siemens Healthcare, Malvern, PA

⁵Division of Medical Physics, University of Leeds

⁶Department of Cardiology, Zena and Michael A. Weiner Cardiovascular Institute and
Marie-Josée and Henry R. Kravis Cardiovascular Health Center, Icahn School of
Medicine at Mount Sinai, New York, NY

: Division of Medical Physics, University of Leeds

Corresponding Author:

Zahi A. Fayad, PhD

Director, Translational and Molecular Imaging Institute

Icahn School of Medicine at Mount Sinai

One Gustave L. Levy Place, P. O. Box 1234

New York, NY 10029; USA

E-mail: zahi.fayad@mssm.edu

Abstract:

Purpose: To evaluate the effect of attenuation of MR coils on quantitative carotid PET/MR exams. Additionally, to develop and evaluate automated attenuation correction method for flexible carotid MR coils was developed and evaluated.

Methods: The attenuation of the carotid coil was measured by imaging a uniform water phantom injected with 37 MBq of 18F-FDG in a combined PET/MR scanner for 24 minutes with and without the coil. In the same session, an ultra-short echo time (UTE) image of the coil on top of the phantom was acquired. Using a combination of rigid and non-rigid registration, a CT-based attenuation map was registered to the UTE image of the coil for attenuation and scatter correction. After phantom validation, the effect of the carotid coil attenuation and the attenuation correction method were evaluated in five subjects.

Results: Phantom studies indicated that the overall loss of PET counts due to the coil was 6.3% with local region-of-interest (ROI) errors reaching up to 18.8%. Our registration method to correct for attenuation from the coil decreased the global error and local error (ROI) to 0.8% and 3.8%, respectively. The proposed registration method accurately captured the location and shape of the coil with a maximum spatial error of 2.6 mm. Quantitative analysis in human studies correlated with the phantom findings, but was dependent on the size of the ROI used in the analysis.

Conclusions: MR coils result in significant error in PET quantification and thus attenuation correction is needed. The proposed strategy provides an operator-free method for attenuation and scatter correction for a flexible MRI carotid surface coil for routine clinical use.

Keywords: PET/MRI, Automatic Attenuation correction, Flexible MRI coils, Carotid Imaging

Introduction:

Attenuation of 511 keV photons is a physical effect that degrades the quantitative accuracy of positron emission tomography (PET) images. A new source of attenuation only relevant in PET/MR imaging is that of MR surface coils, such as cardiac or carotid surface coils, that are crucial for magnetic resonance (MR) acquisitions. The design of non-attenuating MR coils has proved difficult with even PET-optimized coils inducing significant quantitative errors in human studies (Paulus *et al.*, 2012; Fürst *et al.*, 2014). Therefore, attenuation correction for such coils, currently not included in the system standard reconstruction, is critical for accurate PET quantification.

Successful attenuation correction for MR hardware and coils requires that an attenuation map containing the correct attenuation factors for the object is available. Furthermore, to apply such attenuation maps, the object has to be accurately localized in the field of view (FOV). For rigid MR coils, including the head and neck coil or the spine coil, the position in the FOV is static allowing for the use of a static attenuation map to correct for their attenuation. Flexible surface coils, on the other hand, change their position and shape between imaging sessions and thus a fixed attenuation map is not a feasible solution.

The use of MR imaging could be utilized to detect the position of flexible coils and other MR hardware in the FOV to allow for registration of a pre-computed attenuation map. Such localization could be achieved by either placing MR visible fiducial markers on the outer surface of the coil or by direct imaging of some of the components of the coil using specialized sequences, such as the ultra-short echo time sequence (UTE) (Paulus *et al.*, 2012). Fully automatic algorithms have been proposed for attenuation correction using fiducial markers (Kartmann *et al.*, 2013; Eldib *et al.*, 2014), however, only manual approaches have been developed for the UTE, which makes the method currently impractical in clinical routine (Paulus *et al.*, 2012; Kartmann *et al.*, 2013). The goal of this study is to develop an automated approach that utilizes UTE MRI to correct for the attenuation of flexible coils.

The use of the UTE to localize coils in the FOV may be more desirable than fiducial markers based localization. Fiducial markers based localization requires modifying the coil by adding additional markers, which will appear in some MR studies

and might interfere with the clinical reading. Furthermore, these markers must always stay on the coil and if they are removed for any reason, a new attenuation map must be re-generated to establish spatial correspondence between the markers in the attenuation map and their physical position (Ferguson *et al.*, 2014). Finally, fiducial markers based registration relies on the correspondence between a very small number of points placed outside of the coil and thus the resultant registration might not capture the actual deformation of the coil (Eldib *et al.*, 2014).

The sensitivity of UTE to measure signal from the structural components of the coils was previously investigated and it was shown that polyethylene-based and some polycarbonate-based materials exhibit a measurable signal (Horch *et al.*, 2010; Marjanska *et al.*, 2008; Springer *et al.*, 2008). In this study we exploit the visibility in UTE MRI acquisitions of the materials used in a specialized neck coil for carotid imaging.

In this study, the effect of attenuation of MR coils was evaluated for carotid PET/MR imaging both in phantoms and in human studies. Moreover, an automatic, attenuation correction method was developed to correct for the attenuation of a flexible carotid coil. The attenuation correction method uses the UTE MRI acquisition to localize the coil in the FOV. Then, using both rigid and non-rigid registration, a pre-computed attenuation map is registered to the UTE image of the coil. Phantom studies were conducted to show feasibility of the attenuation correction algorithm. Preliminary clinical evaluation of the technique was also tested in five subjects using a simultaneous PET/MR scanner.

Materials and Methods:

Carotid Coil:

The Machnet carotid coil (Machnet BV, Roden, The Netherlands) is a two sided, 4-channel phased array surface carotid coil. The effective length of the coil in the anterior posterior direction is 105 mm, and the width is 60 mm. This coil connects to the scanner via very flexible cables making the reproducible placement of the coil in the same position in the FOV difficult. The coil is comprised of a rigid housing for the pre-amplifier electronics, made of Polyoxymethylene; the semi-flexible receiver elements, which can bend around the patient's neck for improved MR imaging are housed in an ethylene propylene diene monomer rubber cushion. **Figure 1** shows one side of the coil and the direction of the motion of the flexible part of the coil.



Fig 1: Images of the coil flat and bent.

UTE Acquisition:

Direct imaging of coil components used a 3D dual echo UTE sequence (TE1=0.07 ms, TE2=2.46 ms, TR = 11.94 ms, flip angle = 10°, FOV = 300 x 300 x 300 mm³, 192 x 192 x 192 voxels, 1.56 x 1.56 x 1.56 mm³ isotropic resolution, acquisition time = 100 s) to localize the coil in the FOV. **Figure 2** shows a typical first echo UTE

image of the coil and its correspondence to the computed tomography (CT) image of the coil in the top panel. Moreover, a sample first echo UTE image *in vivo* is shown in the bottom panel of **Figure 2**.

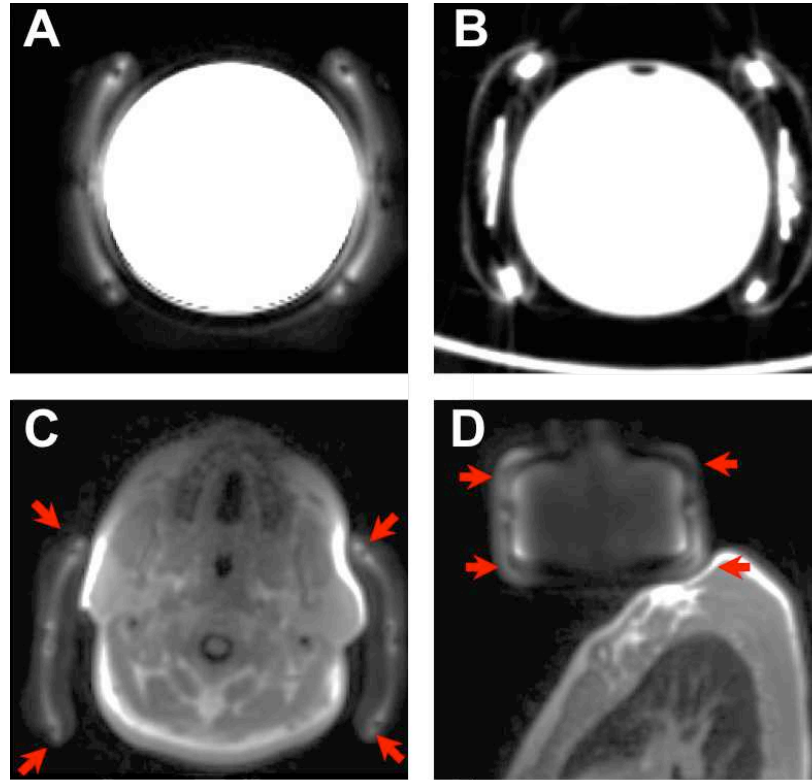


Fig 2: Top panel: a) first echo UTE image and b) the corresponding CT image of the carotid coil on a cylindrical water phantom showing the correspondence between the two images. Bottom panel: c) axial and d) Sagittal views of the first echo image in a human study showing the coil highlighted by the red arrows.

PET/MR Imaging:

All PET/MR studies were conducted on the Siemens Biograph mMR (Siemens Healthcare, Erlangen, Germany) (Delso *et al.*, 2011). The spatial resolution of the scanner is 4.3 mm (FWHM) at 1 cm offset from the center of the FOV (Delso *et al.*, 2011). All PET reconstructions in this study were performed offline using dedicated reconstruction software provided by the manufacturer (e7-tools for Siemens Biograph mMR VB18P). PET emission data was corrected for dead time, attenuation, scatter, randoms and normalization. PET images were reconstructed using the ordinary Poisson ordered subsets expectation maximization algorithm using 3 iterations and 21 subsets.

The resultant PET images had a matrix size of 344x344x127 with a resolution of 2.09x2.09x2.03 mm³. Post-reconstruction smoothing was not applied to the PET images.

CT Imaging and Attenuation Map Generation:

CT-based attenuation maps were used for the coil and the phantom. CT scans were acquired on the Biograph mCT (Siemens Healthcare, Knoxville, TN, USA) using peak tube voltage of 140 kVp. Images were reconstructed on a 512x512x315 with voxels of 1.52x1.52x1.00 mm³. The CT images were smoothed using a 2 mm Gaussian smoothing filter before applying a bilinear transformation to transform Hounsfield units to attenuation coefficients at 511 keV (Carney *et al.*, 2006). The attenuation maps were re-sampled to match the PET image dimensions. Finally, the maps were clipped at 0.02 cm⁻¹ and 0.12 cm⁻¹, as previously described (Eldib *et al.*, 2014; Aklan *et al.*, 2013). This clipping is useful to mitigate overestimation of the attenuation coefficients at 511keV that originate from metal artifacts in the CT images.

Registration Procedure:

The attenuation correction procedure is summarized in **Figure 3**. Firstly, because the coil was only visible in the first echo UTE image, the second echo image was used to remove the subject and the MR markers so that they do not interfere with the registration. This was done automatically by thresholding the 2nd echo image at background level and morphologically closing the resultant image to generate a binary mask that was then filtered from the 1st echo image. The coil image was then divided into two sides in the axial direction at the center of mass of the image (in the X direction) for subsequent registration of each side of the coil separately. The registration procedure was initialized by a 3-dimensional (3D) normalized mutual information maximization rigid registration of the attenuation map to the UTE image of the coil over six degrees of freedom (3 translation and 3 rotation). Then, the diffeomorphic demons algorithm as implemented in the National Library of Medicine Insight Segmentation and Registration Toolkit (ITK) was used to warp the attenuation map non-rigidly (Vercauteren *et al.*, 2009). The demons algorithm is a popular iterative deformable image registration algorithm that estimates the deformation between images caused by edge based forces (Thirion, 1998). The demons algorithm requires regularization and in its simplest form, Gaussian

smoothing of the transformation field is used. The use of diffeomorphic regularization, however, has been shown to produce non-folding transformation fields, which are physically unlikely to occur (Vercauteren *et al.*, 2009). More importantly, diffeomorphic regularization preserves the topology of objects in images, which is important for our current registration problem. The rigid and non-rigid registration steps were then repeated for the other side of the coil. To estimate the values of the attenuation map at the registered position, 3rd order b-spline interpolation was used. After registration, the resultant left and right attenuation maps of the coil were combined into a single coil attenuation map for use in system standard PET reconstruction to correct for attenuation and scatter due to the coil.

Phantom Evaluation of the Coil Attenuation:

To study attenuation of the carotid coil, a uniform water phantom (diameter = 12 cm) was injected with 37 MBq of 18F-FDG and scanned on the PET/MR for 24 minutes (3 times longer than the standard patient scan time). Eight minutes after the completion of the first PET acquisition, the same phantom was scanned for the same duration with the coil present. Decay correction was applied to account for the 18F-FDG decay between acquisitions. A CT-based attenuation map of the phantom was used in all reconstructions to ensure that any measured differences in the reconstructed PET images are solely due to the coil attenuation and not errors in the phantom attenuation map. The attenuation map was registered to the non-attenuation corrected PET emission image using rigid normalized mutual information registration.

The PET emission data collected without the coil (i.e. ground truth) was reconstructed using a phantom only attenuation map to serve as ground truth. Subsequently, the acquisition done with the coil present was reconstructed without accounting for attenuation from the coil (i.e. using only a registered phantom attenuation map) in the overall attenuation map. When the resultant image is compared to the ground truth, the effect of the coil on quantification can be investigated. Finally, the same data set was reconstructed with a coil attenuation map registered to UTE image to test the feasibility of the proposed attenuation correction approach.

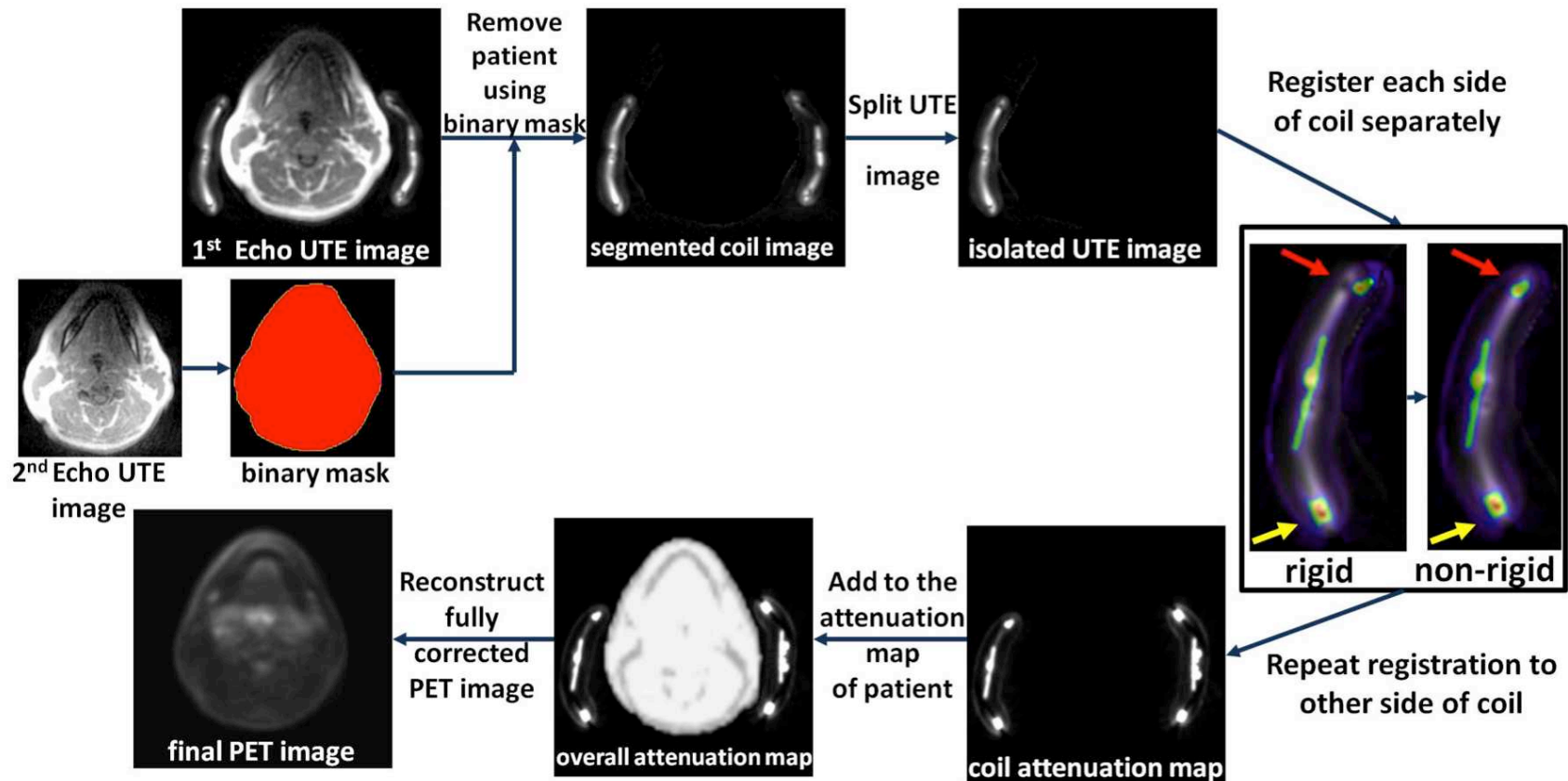


Fig 3: Flow chart for the registration algorithm. After the UTE acquisition, the coil was segmented by using a mask generated by thresholding and morphological closing of the 1st echo UTE image. The resultant image was then split at the center of mass for subsequent rigid and non-rigid registration of the attenuation map of each side of coil separately. The registration procedure was repeated for the other side of coil and then added to the system generated attenuation map to reconstruct the final fully corrected PET image.

Human Studies:

This study was approved by the local Institutional Review Board and all subjects provided informed consent. Five human subjects (4 females and 1 male) with risk factors for cardiovascular disease were injected with ^{18}F -FDG. The mean injected dose was 392 ± 129 MBq. The duration between ^{18}F -FDG injection and scan time (circulation time) was 96.6 ± 2.1 minutes. PET data was acquired in a single bed position centered on the carotid bifurcation for 8 minutes, with the carotid MRI surface coil, followed by another acquisition of a single bed position for 8 minutes, without the coil. The scans were performed in this order to minimize motion between scans during the removal of the coil from the subject. Attenuation correction for the patient was performed by segmentation of 3D Dixon-VIBE (volume-interpolated breath-hold examination) MR images into a 4-segment attenuation map (soft tissue = 0.1000 cm^{-1} , fat = 0.0854 cm^{-1} , lung 0.0224 cm^{-1} , and air 0.0000 cm^{-1}), as is standard on the scanner (Martinez-Moller *et al.*, 2009). UTE images were collected immediately after the PET acquisition, while time of flight MR angiography sequences (TE = 3.69 ms, TR = 23 ms, $256 \times 256 \times 256$ voxels with sizes of $0.7 \times 0.7 \times 1$ mm, acquisition time 13:29 min) were collected simultaneously with the PET scan for anatomical reference for the carotids.

Evaluation of the Registration Method:

To investigate accuracy of the coil registration, the method that was previously presented by Kartmann *et al.* was used in this study (Kartmann *et al.*, 2013). Four markers (MR SPOTS MRI Skin Marker, ref. no. 185; Beekley Medical, Bristol, CT, USA) visible in both MR and CT, with diameter of 8 mm were placed on the outer surface of the coil. Following the registration procedure, the markers were localized in both the UTE image and the registered attenuation map to measure the mean squared distance between the markers as a metric for registration accuracy over all subjects.

Additionally, to evaluate if the registration procedure preserves the shape and the attenuation coefficients of the CT map, the percent difference was computed between the attenuation map before and after registration. Moreover, visual inspection of the attenuation maps was performed to evaluate the shape of the deformed attenuation map.

Clinical Evaluation of the Attenuation Correction Method:

PET acquisitions of patients were reconstructed with the same parameters as the phantom scan. Data collected without the coil was considered ground truth. PET emission data collected with the coil present was either reconstructed with or without the coil attenuation map included in the overall attenuation map to investigate the effect of the coil and the feasibility of our approach for attenuation correction in patient studies.

Image Analysis:

Phantom Data

Global quantitative analysis for the phantom data was done by investigating the average activity in a large ROI that enclosed the entire phantom. Furthermore, ROI analysis was also conducted to quantify local errors from attenuation of the coil using a 2 cm ROI placed 2 cm and 5 cm away from the coil to investigate the attenuation effects of the coils at a depth range similar to the position of carotid arteries in humans. The size of the ROI was chosen so that it represents the size of the carotid artery lumen and the vessel wall that might contain plaques (El Aidi *et al.*, 2009).

Human Data

Quantitative comparisons in the human studies were carried out both globally and locally. Global analysis was done using a large ROI around the neck of the patient. Additionally, 2 cm circular ROIs centered on both carotids was used for local analysis. Data are presented as mean over all subjects \pm standard deviation. Statistical analyses to identify the significance of the attenuation of the coil as well as our attenuation correction method in human studies were performed using paired t-tests between data reconstructed with and without the coil in the overall attenuation map and compared to the ground truth (no coil scan). Statistical significance was considered for $p < 0.01$.

Results:

Coil attenuation map:

Figure 4 shows a sample coronal slice of the CT-based attenuation map before clipping of the attenuation coefficients and the corresponding image. The plastic housing in the coil has the highest attenuation, while the foam part of the coil has the lowest. The plastic housing around the electronics has attenuation coefficients between 0.10 cm^{-1} and 0.18 cm^{-1} . The outer foam shell of the coil has attenuation coefficient of about 0.02 cm^{-1} while the foam and polyester foam has negligible attenuation.

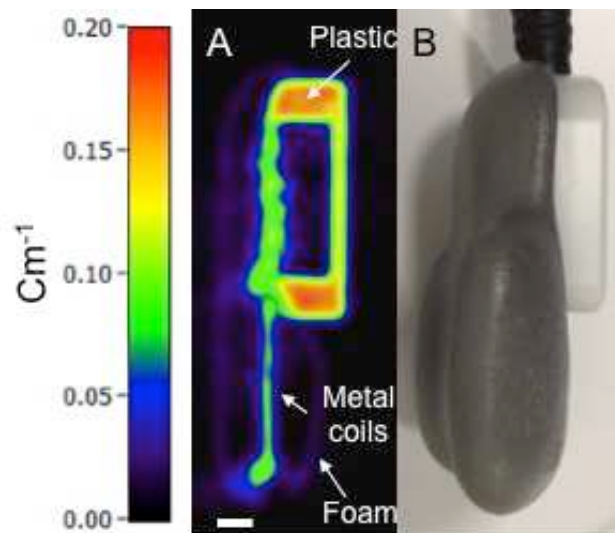


Fig 4: *A) Sample plane across the attenuation map of the carotid coil. The plastic housing around the coil is the most attenuating part of the coil followed by the metallic components and the foam. B) Corresponding image of the coil. Scale bar is 1 cm.*

Quantification of the coil attenuation:

The experimental setup of the phantom with the coils placed around it as placed in the scanner is shown in **Figure 5A**. Phantom studies indicated that the overall loss of PET counts (i.e. net true events) due to the carotid coil was 6.3%. This global loss of counts, however, was not uniform in all areas with the error reaching up to 11.9% in some axial planes. Furthermore, local quantitative differences in the 2 cm ROI reached an underestimation of 18.8% and 13.4% in the ROI placed 2 cm and 5 cm away from the surface of the coil as shown in **Figure 5B**. Attenuation correction for the coil was necessary given the high error that was produced due to the presence of the coil in the PET FOV.

Attenuation correction for the carotid coil using our proposed method:

Having established that the attenuation correction was required for the carotid coil, attenuation correction was performed using the proposed registration method. The overall computation time for the coil isolation and image registration procedure for both sides of the coil was 242 seconds. Following attenuation correction for the coil, the global difference in quantification was 0.8%. The largest error that measured in the ROIs placed 2 cm and 5 cm away from the coil was 3.8% and 3.7% respectively following attenuation correction.

Evaluation of the Registration Method:

The coil was visible in the UTE images of all patients that were scanned with the coil in the FOV. **Figure 5C** shows the organization of the markers on the outer surface of the coil. A summary of the results of registration accuracy is shown in **Table 1**. The average error for marker 1 and 2 (which quantify the error in the rigid transformation) was 1.9 mm. For markers 3 and 4, which quantify the error in the non-rigid part of the algorithm, the error was 2.5 mm.

Marker	Error	Error
	Rigid transformation	Non-rigid transformation
1	1.8±0.3	1.8±0.4
2	2.1±0.4	2.2±0.7
3	4.5±1.6	2.6±1.1
4	4.3±2.3	2.4±0.9

Table 1: Summary of the mean squared error between the UTE and the resultant attenuation map registered by rigid and non-rigid registration.

The percent differences for the CT map before and after registration was computed to investigate if the registration procedure affected the overall attenuation coefficients for the CT map. We found that the difference was about 2.0% for the left side and 1.9% for the right side suggesting that the difference is negligible. Moreover, visual inspection did not reveal unphysical deformations following the registration process.

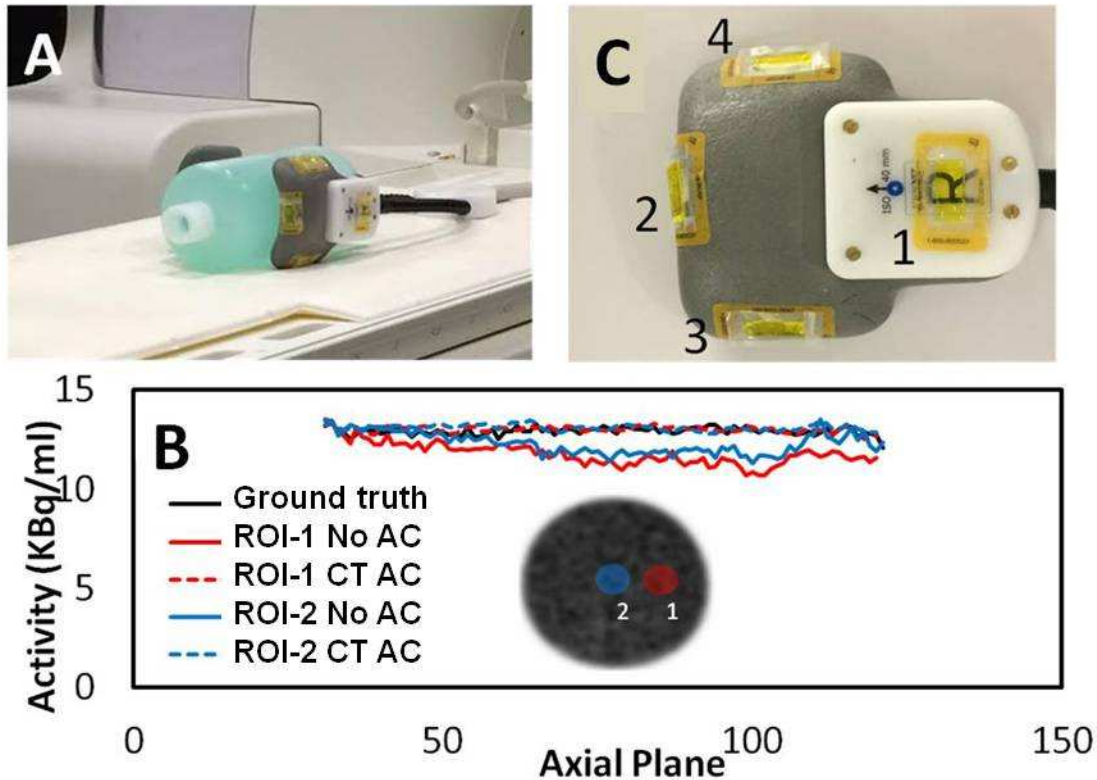


Fig 5: A) Image of the phantom acquisition setup on the scanner. B) A close-up image to show the placement of the markers used in the evaluation of the registration accuracy. C) Plot of the mean activity within a ROI over all axial planes that contained the phantom in the PET image.

Clinical Evaluation of the Attenuation Correction Method:

Figure 6A shows a line profile across the neck of the patient that plots the activity distribution along the line shown in the figure insert. ROI around the neck of the subject, which was the active area of the coil, was used for a global analysis. In the neck region, the coil resulted in significant attenuation of $9.1\% \pm 1.7\%$ ($p < 0.01$). Following attenuation correction for the coil, the measured difference from the reconstructed images was $1.6\% \pm 2.7\%$ ($p = 0.13$) in all five subjects (**Figure 6B**).

In the 2 cm ROIs around the left and right carotids the measured reduction of quantification was $9.6\% \pm 3.5\%$ ($p < 0.01$) and $8.2\% \pm 0.5\%$ ($p < 0.01$). Following attenuation correction the measured activity was underestimated by $0.3\% \pm 2.3\%$ ($p = 0.40$) for the left carotid and overestimated by $2.1\% \pm 3.7\%$ ($p = 0.14$) for the right carotid (**Figure 6C**).

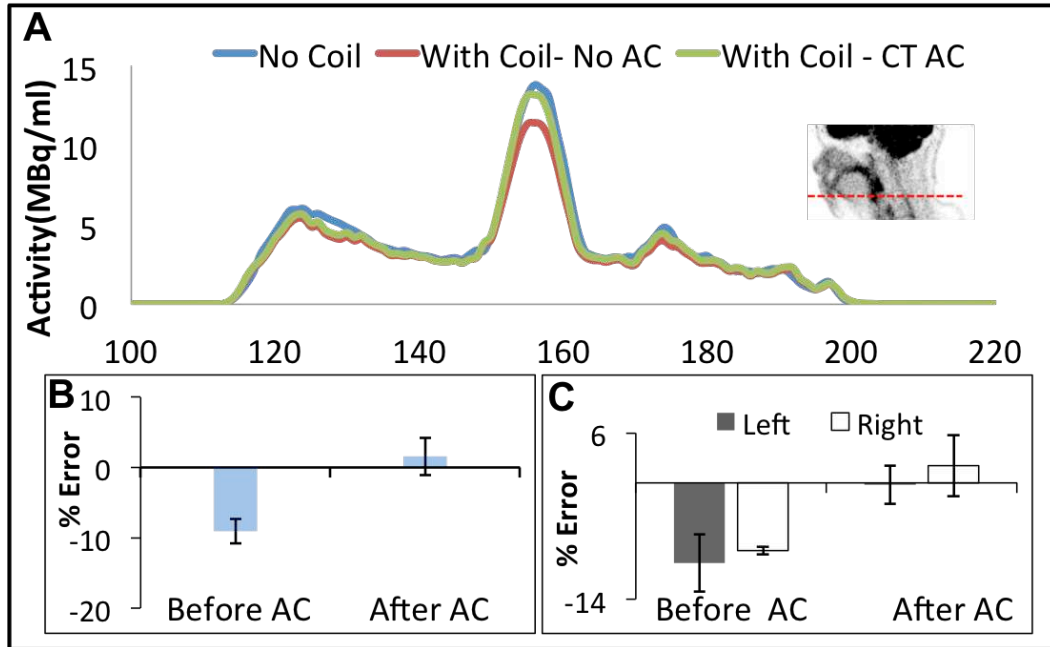


Fig 6: Sample line profile across the neck of the patient showing the effect of attenuation (with coil- no AC) as well as after attenuation correction with the proposed method (with coil- CT AC) compared to the no coil scan, which serves as ground truth. The insert shows the location of the line profile (A). Bar plot showing measured error for the large ROI around the neck (B) and the 2 cm ROI around the left and right carotid (C).

Discussion:

In this study, the effect of a carotid coil was evaluated both in phantom studies as well as *in vivo*. It was found that the presence of the coil resulted in significant attenuation and thus attenuation correction was needed to achieve accurate quantification. To this end, an automatic algorithm was proposed for attenuation correction for flexible coils in combined PET/MR that utilized UTE MRI. Previous studies utilized UTE MRI for attenuation correction with only manual and rigid registration (Paulus *et al.*, 2012). In this study a fully automatic and non-rigid registration was used, making the proposed method feasible for routine clinical use. The proposed attenuation correction strategy presented in this study for the carotid coil could be expanded to other flexible coils, provided they are made from UTE visible materials, because such coils deform in a similar fashion where rigid registration would capture the bulk motion while non-rigid registration better describes the flexure motion of such coils.

This study showed that neglecting the attenuation of flexible coils, in this case a dedicated carotid surface coil, which are needed for high resolution MR imaging, had a significant adverse effect on PET quantification. With results from this study and previous coil attenuation studies, it is evident that hardware attenuation correction is required for combined PET/MR to reach its potential as an accurate quantitative diagnostic tool (Kartmann *et al.*, 2013; Delso *et al.*, 2010; Eldib *et al.*, 2014; MacDonald *et al.*, 2011; Paulus *et al.*, 2012; Dregely *et al.*, 2014).

The utility of UTE MRI for the purpose of attenuation correction for MRI hardware has been of recent interest, however, clinically feasible algorithms that do not require user intervention have not yet been developed. Previously a manual, rigid algorithm was used for the body matrix coil (Paulus *et al.*, 2012). Most recently, UTE based localization was tested also to localize the headphones used in head PET/MR scans, however, a sufficient signal was not emitted from the headphones and thus an algorithm was not developed (Ferguson *et al.*, 2014).

The diffeomorphic demons algorithm used in our study has been used previously in the registration of images of different contrast in several previous studies (Archip *et al.*, 2007; Janssens *et al.*, 2011). Similar to our findings in Table 1, the misregistration error reported in the study by Archip *et al.* was 3.04 mm.

There are several advantages and disadvantages to both MRI based localization methods. Fiducial markers may interfere with some MR images that are generated with the coil present and the physician must be aware of their presence before reading the data. Furthermore, the markers must always remain on the coil and if they are detached then a new attenuation map must be re-generated making it inconvenient for routine use (Ferguson *et al.*, 2014). Fiducial markers based registration utilizes a very limited number of scattered corresponding points between the MR image and the attenuation map placed mostly on the outer surface of the coil and thus interpolation between those points must be used to estimate the position of the coil in the FOV in between those markers. It was shown recently that significant mis-registration could occur depending on the type of interpolation used, which could lead to erroneous attenuation correction and quantitative errors in the reconstructed PET image (Eldib *et al.*, 2014). Direct imaging of the coil, such as the one used in this study, where large sections of the coil itself are imaged could

reduce the need for such sparse interpolation. A current limitation for the UTE approach on the PET/MR scanner used in this study is that it is restricted to a small FOV, but could be modified to include a wider FOV at the expense of increased scan time (Togao *et al.*, 2010). The duration of the UTE sequence used in this study is only 100 seconds and it is included in the clinical protocols for PET/MR imaging of the carotids, thus separate UTE imaging of the coil would not be necessary (Delso *et al.*, 2011).

The use of CT-based attenuation maps, which has been the clinical standard for attenuation correction in PET/CT scanners, was extended to attenuation correction for MR coils (Townsend, 2008; Carney *et al.*, 2006). Findings in this study suggest that CT-based attenuation maps that were generated from CT images using the conventional bilinear transformation (Carney *et al.*, 2006) may be sufficient for hardware attenuation correction of small coils such as the one used in this study. Our findings are consistent with recent reports that used the same transformation to successfully correct for the attenuation of MR coils (Tellmann *et al.*, 2011; Paulus *et al.*, 2012; Kartmann *et al.*, 2013; Aklan *et al.*, 2013; Eldib *et al.*, 2014; Dregely *et al.*, 2014).

The spatial accuracy of the registration algorithm was investigated in this study in five human studies using a method previously proposed by Kartmann et al (Kartmann *et al.*, 2013). An advantage of this approach is that it allows for the investigation of the spatial accuracy at various realistic and clinically applicable positions of the coil at relevant noise levels. A small error was found following non-rigid registration (max of 2.6 mm), which is below the spatial resolution of the scanner indicating that the accuracy is sufficient for attenuation correction. Several studies have evaluated the effect of mis-registration of the attenuation maps to their actual position for several rigid and flexible coils and it was concluded that positional error on the scale of 3 mm or 4 mm depending on the size of the coil do not introduce significant changes in quantification (Delso *et al.*, 2010; Paulus *et al.*, 2013; Eldib *et al.*, 2014).

Clinical evaluation of hardware attenuation correction is a challenging task. In clinical studies, unlike phantom scans, the tracer is re-distributed between neighboring tissues during and in between acquisitions, making it difficult to assume that any measured quantitative difference is solely due to the attenuation of the coil. It was recently shown however that the standard uptake value does not change significantly over

the short duration used in this study (Bucerius *et al.*, 2014). Furthermore, motion between scans, partial volume effects, as well as noise could have a large contribution to the measured quantitative differences.

Conclusion:

In this study, the effect of attenuation of flexible coils was investigated for carotid PET/MR imaging. It was found that such coils resulted in a significant reduction in quantification and thus attenuation correction was required. To this end, a fully automatic algorithm was developed for attenuation correction for the carotid coils by registering a pre-computed CT-based attenuation map to the UTE MR image of the coil. Firstly, we showed that ignoring the attenuation of the coil led to large quantitative errors. In addition, we demonstrated quantitatively in phantoms that the attenuation of the coil could be corrected using the proposed method with high accuracy. Finally, preliminary evaluation of the technique was demonstrated in five human PET/MR studies, showing reduction in the difference between activity quantification with the MR coil and without when our correction method was used. Taken together, this method could be translated to routine clinical PET/MR exams of the neck.

Acknowledgements:

The authors would like to thank Siemens Healthcare for its technical support. This work is supported in part by a grant from the National Institute of Health, National Heart Lung and Blood Institute, and National Center for Advancing Translational Science (NIH/NHLBI R01 HL071021, R01 HL078667 and NIH/NCATS CTSA UL1TR000067) (ZAF). Dr Tsoumpas visit was in part supported by the Whitehead Travel Scholarship, School of Medicine, University of Leeds.

References:

- Aklan B, Paulus D H, Wenkel E, Braun H, Navalpakkam B K, Ziegler S, Geppert C, Sigmund E E, Melsaether A and Quick H H 2013 Toward simultaneous PET/MR breast imaging: systematic evaluation and integration of a radiofrequency breast coil *Med Phys* **40** 024301
- Archip N, Tatli S, Morrison P, Jolesz F, Warfield S K and Silverman S 2007 Non-rigid registration of pre-procedural MR images with intra-procedural unenhanced CT images for improved targeting of tumors during liver radiofrequency ablations *Medical image computing and computer-assisted intervention* **10** 969-77
- Bucerius J, Mani V, Moncrieff C, Machac J, Fuster V, Farkouh M E, Tawakol A, Rudd J H and Fayad Z A 2014 Optimizing 18F-FDG PET/CT imaging of vessel wall inflammation: the impact of 18F-FDG circulation time, injected dose, uptake parameters, and fasting blood glucose levels *European journal of nuclear medicine and molecular imaging* **41** 369-83
- Carney J P, Townsend D W, Rappoport V and Bendriem B 2006 Method for transforming CT images for attenuation correction in PET/CT imaging *Med Phys* **33** 976-83
- Delso G, Fürst S, Jakoby B, Ladebeck R, Ganter C, Nekolla S G, Schwaiger M and Ziegler S I 2011 Performance measurements of the Siemens mMR integrated whole-body PET/MR scanner *J Nucl Med* **52** 1914-22
- Delso G, Martinez-Moller A, Bundschuh R A, Ladebeck R, Candidus Y, Faul D and Ziegler S I 2010 Evaluation of the attenuation properties of MR equipment for its use in a whole-body PET/MR scanner *Physics in medicine and biology* **55** 4361-74
- Dregely I, Lanz T, Metz S, Mueller M F, Kuschan M, Nimbalkar M, Bundschuh R A, Ziegler S I, Haase A, Nekolla S G and Schwaiger M 2014 A 16-channel MR coil for simultaneous PET/MR imaging in breast cancer *European radiology*
- El Aidi H, Mani V, Weinschelbaum K B, Aguiar S H, Taniguchi H, Postley J E, Samber D D, Cohen E I, Stern J, van der Geest R J, Reiber J H, Woodward M, Fuster V, Gidding S S and Fayad Z A 2009 Cross-sectional, prospective study of MRI reproducibility in the assessment of plaque burden of the carotid arteries and aorta *Nature clinical practice. Cardiovascular medicine* **6** 219-28
- Eldib M, Bini J, Calcagno C, Robson P M, Mani V and Fayad Z A 2014 Attenuation correction for flexible magnetic resonance coils in combined magnetic resonance/positron emission tomography imaging *Invest Radiol* **49** 63-9
- Ferguson A, McConathy J, Su Y, Hewing D and Laforest R 2014 Attenuation Effects of MR Headphones During Brain PET/MR Studies *Journal of nuclear medicine technology* **42** 93-100
- Fürst S, Souvatzoglou M, Martinez-Moller A, Schwaiger M, Nekolla S G and Ziegler S I 2014 Impact of flexible body surface coil and patient table on PET quantification and image quality in integrated PET/MR *Nuklearmedizin. Nuclear medicine* **53**
- Horch R A, Wilkens K, Gochberg D F and Does M D 2010 RF coil considerations for short-T2 MRI *Magnetic resonance in medicine : official journal of the Society of Magnetic Resonance in Medicine / Society of Magnetic Resonance in Medicine* **64** 1652-7

- Janssens G, Jacques L, Orban de Xivry J, Geets X and Macq B 2011 Diffeomorphic registration of images with variable contrast enhancement *International journal of biomedical imaging* **2011** 891585
- Kartmann R, Paulus D H, Braun H, Aklan B, Ziegler S, Navalpakkam B K, Lentschig M and Quick H H 2013 Integrated PET/MR imaging: automatic attenuation correction of flexible RF coils *Med Phys* **40** 082301
- MacDonald L R, Kohlmyer S, Liu C, Lewellen T K and Kinahan P E 2011 Effects of MR surface coils on PET quantification *Med Phys* **38** 2948-56
- Marjanska M, Waks M, Snyder C J and Vaughan J T 2008 Multinuclear NMR investigation of probe construction materials at 9.4T *Magnetic resonance in medicine* **59** 936-8
- Martinez-Moller A, Souvatzoglou M, Delso G, Bundschuh R A, Chefd'hotel C, Ziegler S I, Navab N, Schwaiger M and Nekolla S G 2009 Tissue classification as a potential approach for attenuation correction in whole-body PET/MRI: evaluation with PET/CT data *J Nucl Med* **50** 520-6
- Paulus D H, Braun H, Aklan B and Quick H H 2012 Simultaneous PET/MR imaging: MR-based attenuation correction of local radiofrequency surface coils *Med Phys* **39** 4306-15
- Paulus D H, Tellmann L and Quick H H 2013 Towards improved hardware component attenuation correction in PET/MR hybrid imaging *Physics in medicine and biology* **58** 8021-40
- Springer F, Martirosian P, Schwenzer N F, Szimtenings M, Kreisler P, Claussen C D and Schick F 2008 Three-dimensional ultrashort echo time imaging of solid polymers on a 3-Tesla whole-body MRI scanner *Invest Radiol* **43** 802-8
- Tellmann L, Quick H H, Bockisch A, Herzog H and Beyer T 2011 The effect of MR surface coils on PET quantification in whole-body PET/MR: results from a pseudo-PET/MR phantom study *Med Phys* **38** 2795-805
- Thirion J P 1998 Image matching as a diffusion process: an analogy with Maxwell's demons *Medical image analysis* **2** 243-60
- Togao O, Tsuji R, Ohno Y, Dimitrov I and Takahashi M 2010 Ultrashort echo time (UTE) MRI of the lung: assessment of tissue density in the lung parenchyma *Magnetic resonance in medicine : official journal of the Society of Magnetic Resonance in Medicine / Society of Magnetic Resonance in Medicine* **64** 1491-8
- Townsend D W 2008 Positron emission tomography/computed tomography *Semin Nucl Med* **38** 152-66
- Vercauteren T, Pennec X, Perchant A and Ayache N 2009 Diffeomorphic demons: efficient non-parametric image registration *NeuroImage* **45** S61-72